

ARTICLE

Open Access

# Strong interference-based ultrathin conductive anti-reflection coating on metal substrates for optoelectronics

Hongyan Liu<sup>1</sup>, Jingjing Peng<sup>1</sup>, Weiming Liu<sup>1</sup>, Yonglin Wang<sup>1</sup>, Jianhua Wu<sup>1</sup>, Guanli Zhang<sup>1</sup>, Xiaoli Wang<sup>2</sup> and Yue Yan<sup>1</sup>

## Abstract

Anti-reflection layers, which comprise one or more films of dielectric or metallic materials, are widely used in many applications, such as solar cells, to reduce unwanted reflection loss or overcome undesirable color features. Many conventional anti-reflection layers are based on multilayer interference, index matching, surface texturing and plasmonic phenomena. Here, we present a novel paradigm that suppresses the reflection of light from a metallic surface by using an ultrathin, conductive CuO coating. This new anti-reflection concept relies on the strong interference inside the ultrathin, absorptive CuO coating. We derive the optimal conditions for minimal reflectance and expound how the film thickness impacts the reflectance. It is shown that zero reflectance can almost be obtained at a wavelength of *ca.* 550 nm over a wide range of incident angles. As a proof-of-concept experiment, a transparent conductive electrode with a record figure of merit was fabricated based on a CuO/Cu double-layer structure, of which CuO was used to tune the chromaticity of the resultant TCEs and protect Cu from oxidation. This technology has the potential for many applications, especially for photoelectrochemical cells, which can be used to simultaneously enhance the total absorption and reduce the minority charge carrier collection length.

## Introduction

Optical coatings are a key component in a wide variety of optoelectronic devices such as solar cells, photoelectrochemical cells, touch screen displays, and optical filters<sup>1–3</sup>. In most cases, anti-reflection layers (AR) to reduce the undesirable reflected/scattered light loss or an absorber to enhance the optical absorption are needed. Conventional anti-reflection layers are often based on the principle of destructive interference to suppress reflection by stacking alternating transparent dielectrics with high and low refractive indices, with thicknesses of a quarter-wavelength ( $\lambda/4n$ , where  $n$  is the refractive index of the dielectrics). Other approaches include a single-layer

nanoparticle coating<sup>4</sup>, a graded-index coating<sup>5</sup>, and taped nanostructures<sup>6</sup>, where the reduced reflection is induced by multiple scattering and interference of light due to a gradually increasing refractive index towards the substrate surface.

Recently, a novel AR material, namely, an absorbing AR coating (ARC), was proposed based on the absorptive property inside the AR layer. Many ARCs have been studied and utilized due to their unique properties in various fields<sup>4,7–11</sup>. However, the configuration of ARCs usually comprises multiple dielectric/metal film layers or an array of plasmonic metal particles surrounded by dielectric media. Although the suppression of reflection of these ARCs is efficient, the insulating property hinders its application in areas of TCEs or other electrode fabrication. Hence, it is paramount to explore a simple conducting double-layer structure with suppressed reflectivity based on a metal substrate, which can be utilized to fabricate TCEs and photoelectrodes<sup>12,13</sup>.

Correspondence: Hongyan Liu ([liuhongyan10@tsinghua.org.cn](mailto:liuhongyan10@tsinghua.org.cn)) or Xiaoli Wang ([wangxl@nanoctr.cn](mailto:wangxl@nanoctr.cn)) or Yue Yan ([yueyan@biam.ac.cn](mailto:yueyan@biam.ac.cn))

<sup>1</sup>Beijing Engineering Research Centre of Advanced Structural Transparencies for the Modern Traffic System, Beijing Institute of Aeronautical Materials, Beijing 100095, China

<sup>2</sup>CAS Key Laboratory of Nanosystem and Hierarchical Fabrication, National Center for Nanoscience and Technology, Beijing 100190, China

© The Author(s) 2018



**Open Access** This article is licensed under a Creative Commons Attribution 4.0 International License, which permits use, sharing, adaptation, distribution and reproduction in any medium or format, as long as you give appropriate credit to the original author(s) and the source, provide a link to the Creative Commons license, and indicate if changes were made. The images or other third party material in this article are included in the article's Creative Commons license, unless indicated otherwise in a credit line to the material. If material is not included in the article's Creative Commons license and your intended use is not permitted by statutory regulation or exceeds the permitted use, you will need to obtain permission directly from the copyright holder. To view a copy of this license, visit <http://creativecommons.org/licenses/by/4.0/>.

In the past years, Cu-nanowire-based or grid-based TCEs have emerged as promising candidates to substitute for both ITO and Ag nanowire TCEs due to their excellent resistivity ( $1.75 \mu\Omega \text{ cm}$ ) comparable to silver ( $1.65 \mu\Omega \text{ cm}$ ), lower price and more abundant reserves than silver or indium<sup>14–21</sup>. However, the actual application of Cu-nanowire-based or grid-based TCEs have been hampered owing to two limiting factors, namely, the undesirable color induced by a parasitic high reflection of Cu nanowires or grids and the easy oxidation property, especially upon exposure to humidity or under the influence of Joule heating. Herein, we propose using an ultrathin-conducting absorptive layer to suppress the reflection of the Cu substrate (absorption enhancement of the absorptive layer) and provide the optimized design parameters. The underlying mechanism of the AR effect was elucidated in detail and is universally suitable for other metal substrates. As a proof-of-concept experiment, CuO was employed as an efficient AR layer for Cu substrates, and a CuO/Cu/CuO-sandwich structure was utilized to fabricate TCEs. The ultrathin CuO film in this configuration performs two functions, namely, it acts as an AR layer to suppress the reflection of the lower Cu grids and as a protective layer to prevent the Cu grids from oxidation. As a result, the visibility of the grid lines in the grid-based TCEs was remarkably reduced, and the stability of the resultant TCEs was significantly enhanced. Moreover, Cu-grid TCEs with a total transmittance of 92–97% and sheet resistance of  $4\text{--}40 \Omega \text{ sq.}^{-1}$  can be obtained from the transmittance enhancement (increase by  $\sim 8\%$ ) of a polyethylene terephthalate (PET) substrate after coating with AR layers. The total performance is far superior to that of commercial ITO ( $R_s = 10 \Omega \text{ sq.}^{-1}$ ,  $T = 85\%$ ) and others.

## Materials and methods

### Simulations

Reflectance simulations of an air/absorptive layer/Cu three-layer structure were carried out according to Eq. (1). An optical simulation for the design of AR layers (AR) was performed by employing a transfer matrix method (TMM), which allows us to calculate the amplitude of the electromagnetic wave at each interface of a multilayer and to obtain the transmittance ( $T$ ) and reflectance ( $R$ ) of a specific stack. For the transmittance and reflectance simulations on PET, layers with refractive indices of 1.46 ( $\text{SiO}_2$ ) and 2.31 ( $\text{TiO}_2$ ) were used. To optimize the layer thickness, we performed a global search and then minimized/maximized the reflectance/transmittance value at  $\lambda = 550 \text{ nm}$  or the averaged reflectance/transmittance value for a spectral range of 380–780 nm for a given structure. The optimal thicknesses are compiled in Table 1S.

### Film deposition

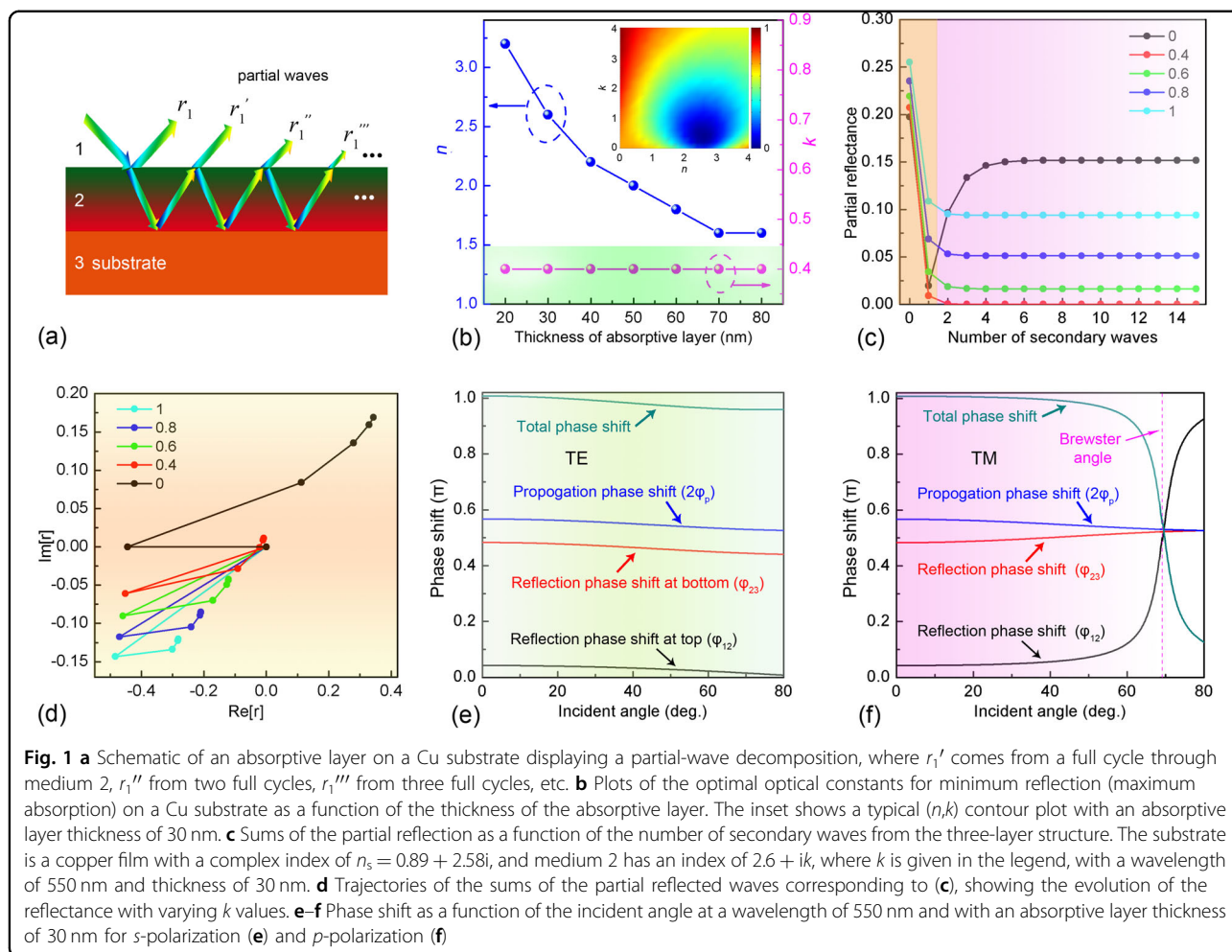
Commercially available PET substrate, with both sides coated with an acrylate hard coating and with a thickness of *ca.* 125  $\mu\text{m}$ , was used to deposit AR layers and sandwiched conducting layers. All of the films were coated by using a homemade roll-to-roll magnetron sputtering (MS) machine, which contains three chambers. Prior to AR layer deposition, the PET substrate was pretreated on-line with oxygen and argon plasma exposure in order to clean the PET surface and enhance the adhesion between the PET substrate and the above-coated films. The AR layers were composed of six alternating silicon oxide ( $\text{SiO}_2$ ) and titanium oxide ( $\text{TiO}_2$ ) layers and was rolled forward and backward three times to complete the AR layers. The targets for the  $\text{SiO}_2$  and  $\text{TiO}_2$  films were pure silicon (with purity of 99.99%) and ceramic titanium oxide (with purity of 99.95%), respectively. After AR layer deposition, the sandwiched conducting layers, consisting of two copper oxide (CuO) layers (with thicknesses of *ca.* 30 and 35 nm for the upper and lower layers, respectively) and one copper layer (with a thickness of *ca.* 300 nm), were coated on one side of the AR layer, which was also exposed to oxygen plasma before the deposition of the conducting layer to enhance the adhesion.

### Photolithography

A photoresist layer (PR-500A, Futurrex) was spin coated on the sandwiched conducting layers rotating at 3000 rpm for 40 s and was then baked for 2 min at 115 °C on a hotplate. Next, a mesh pattern was formed on the photoresist layer by employing UV lithography. The mesh structure in the photoresist layer was formed after the regions that were exposed to UV light were removed with a developer (RD6, Futurrex) and then rinsed with distilled water. The samples were then annealed at 110 °C on a hotplate for 5 min to enhance the adhesion of the mesh-structured photoresist on the lower layer. The samples were then wet-etched using a Cu etchant made from 0.1 mol/L copper dichloride ( $\text{CuCl}_2$ ). The feature size of the grid lines could be controlled by varying the etching time. Following the chemical-etching process, the mesh-structured photoresist masking layer was removed with acetone, and the samples were rinsed with ethanol and then distilled water.

### Characterization

The refractive indices of the Cu and CuO films were measured by a spectroscopic ellipsometer (SENTECH), and the phase of the CuO film was characterized by X-ray diffraction with a Rigaku diffractometer (Figure 2S). The reflectance and transmittance spectra were measured with a UV-Vis-NIR spectrophotometer (VARIAN 5000) over a wavelength range of 380 to 780 nm at an interval of 1 nm. The substrate contribution was taken into consideration



in the transmittance measurements, namely, the total transmittance of the substrate and film. A four-point sheet resistance meter (NAGY SD-510) was used to measure the sheet resistance. An X-ray photoelectron spectrometer (XPS, Escalab 250Xi) was employed to evaluate the depth variation of the valence states of the oxygen and copper elements in the copper oxide and copper metal films before and after the durability test. All of the spectra were calibrated with C 1s at 284.5 eV, which originated from adventitious carbon contamination. A constant humidity box was used to carry out durability testing. The topography of the etched grids was measured with atomic force microscopy (NanoScope v7.10).

## Results and discussion

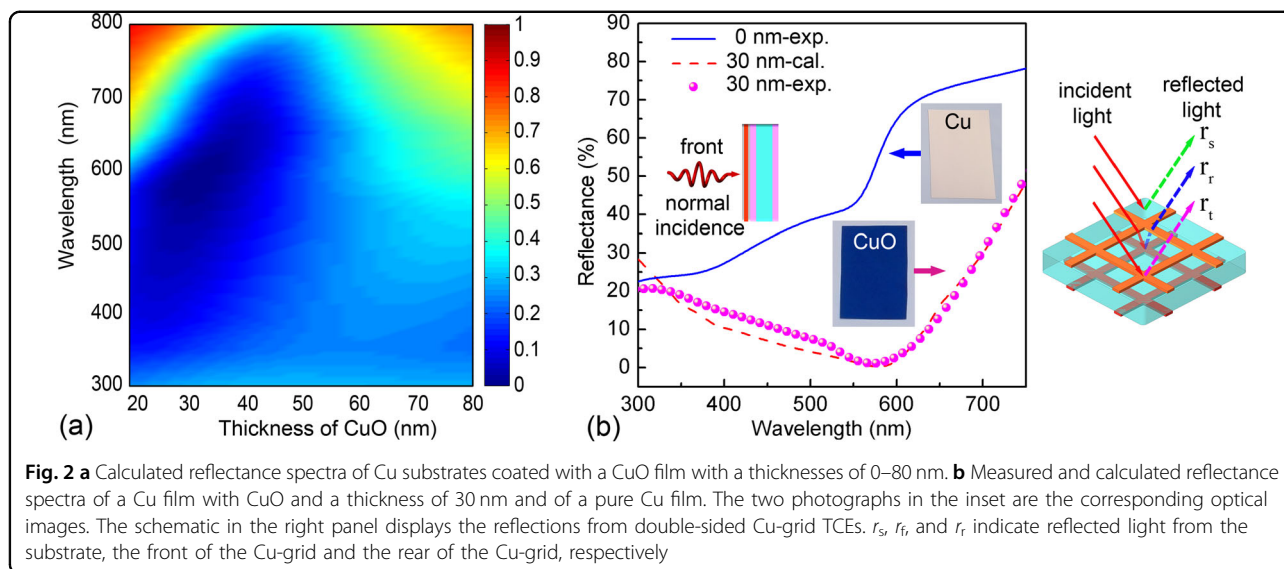
First, an absorptive film with an optimal complex index for a given thickness on a Cu substrate to suppress reflectance was selected. As a model system, and as illustrated in Fig. 1a, we consider a thin homogeneous absorptive layer with a thickness  $d$  and a complex refractive index  $n_2 = n + ik$  coated on a thick Cu film. In this case, the complex index ( $n_2$ ) of the absorptive layer is

optimized for normal incident light at a wavelength of  $\lambda = 550$  nm with various layer thicknesses. The reflection coefficient for transverse-electric ( $s$ -polarized) light at an incidence angle  $\theta_1$  taking multiple internal reflections into consideration is

$$r = \frac{r_{12} + r_{23} e^{2i\beta}}{1 + r_{12}r_{23} e^{2i\beta}} \quad (1)$$

where  $r_{xy} = (p_x - p_y)/(p_x + p_y)$ ,  $p_x = n_x \cos(\theta_x)$ ,  $\beta = (2\pi/\lambda) n_2 d \cos(\theta_2)$  and  $\theta_x = \sin^{-1}(\sin(\theta_1)/n_x)$ , which is the complex-valued form of Snell's law<sup>11</sup>. For transverse-magnetic ( $p$ -polarized) light,  $p_x$  is replaced by  $q_x = n_x/\cos(\theta_x)$ , and the total reflectance is given by  $R = |r|^2$ .

The calculations of reflectivity vs  $(n, k)$  based on the air/absorptive layer/Cu structure are shown in Fig. 1S (see the supporting information) according to Eq. (1). For given thickness and complex index values of the Cu substrate, there is a near-zero reflectivity point of  $(n, k)$  in addition to thicker films over 80 nm, of which an additional minimum appears along the  $n$ -axis due to Fabry–Perot modes. The optimal complex index  $(n, k)$  at a point of



near-zero reflectivity was extracted and plotted in Fig. 1b. Figure 1b clearly shows that the imaginary part remains nearly constant at 0.4 with changes in the thickness, while the real part varies substantially. Considering the application of this structure in transparent conductive films, photovoltaic and photoelectrochemical solar energy conversion, the absorptive layer must be ultrathin, conductive, and photoactive<sup>22</sup>. Accordingly, we chose CuO as an absorptive layer to tune the optical property of the Cu film, with an optical constant of  $n_2 = 2.48 + 0.59i$  at a wavelength of 550 nm (see the supporting information, Fig. 2S), which is very close to the value indicated in Fig. 1b at a thickness of 30 nm and corresponds roughly to  $\lambda/7n$ .

Now, we will explain the underlying mechanism of the reflectance suppression in more detail. Theoretically, when zero reflectance is achieved, the module of the total reflectance efficient is equal to zero (i.e.,  $R = |r|^2$ ). This can only occur when  $r_{12} + r_{23} e^{2i\beta} = 0$ , according to Eq. (1), considering that the denominator of the right term in Eq. (1) is finite. Thus, the following equations can be deduced to satisfy the zero reflectance condition:

$$R_{12} = R_{23} e^{-4\pi nd/\lambda} \quad (2)$$

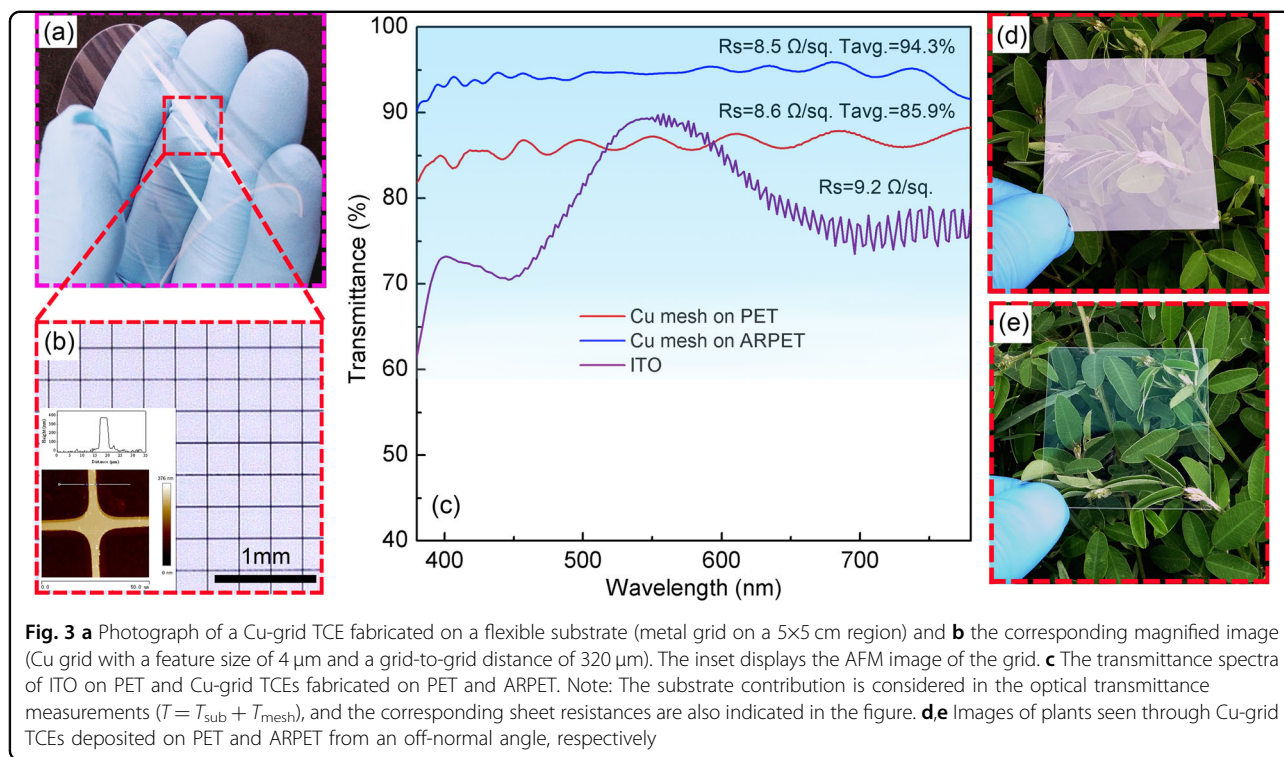
$$\phi_{23} + \phi_{prop.} - \phi_{12} = (2m + 1)\pi \quad (3)$$

where  $R_{12}$  and  $R_{23}$  are the amplitudes of the phases of  $r_{12}$  and  $r_{23}$ , respectively;  $\phi_{12}$  and  $\phi_{23}$  are the phase shift in the interfaces of 1/2 and 2/3, respectively.  $\phi_{prop.}$  is the propagation phase increase in the absorptive layer, and  $m$  is an integer. When the condition defined by these two equations is met, destructive interference in the three-layer structure (Gires–Tournois configuration) occurs.

The physical mechanism of the aforementioned destructive interference can be understood by

investigating the behaviors of partial reflected waves in the Gires–Tournois<sup>11</sup>. Here, we take the case of  $n_2 = 2.6 + ik$ , namely, the case with an absorptive layer thickness of 30 nm on a Cu substrate. The reflectance efficient  $r$  in Eq. (1) is the sum of all of the partial reflected waves, as illustrated in Fig. 1a, i.e.,  $r = \sum r_m$  where  $r_m = t_{12} r_{23}^m r_{21}^{(m-1)} t_{12} e^{2mi\beta}$  for  $m > 0$  and  $r_{xy}^{m=0} = (p_x - p_y)/(p_x + p_y)$ ,  $t_{xy} = 2p_{xy}/(p_x + p_y)$ ,  $p_x = n_x \cos(\theta_x)$ ,  $\beta = (2\pi/\lambda) n_2 d \cos(\theta_2)$ ,  $\theta_x = \sin^{-1}(\sin(\theta_1)/n_x)$  and  $r_0 = r_{12}$ . Here,  $r_0$  is the complex reflection coefficient of the reflected wave from air to the absorptive layer,  $r_m$  is the partial reflected wave that undergoes  $m$  cycles in the absorptive layer. Thus, to see how the total reflectance evolves with secondary waves, we calculated the partial reflectance as a function of the secondary waves, which are plotted in Fig. 1c. In the calculation, the complex index of copper is  $n_s = 0.89 + 2.58i$  at 550 nm, and the absorptive layer has an index of  $n_2 = 2.6 + ik$  with a thickness of 30 nm, where  $k$  varies from 0 to 1. From Fig. 1c, it is clear that the reflectance of  $r_0$  is larger than 0.2 regardless of the  $k$  used. When the first 1–2 secondary waves are taken into consideration, the partial reflectance decreases sharply, even reaching 0 at  $k = 0.4$ . The partial reflectance reaches its final value for all cases, with a loss after considering no more than 4 partial waves.

For the partial waves reflected from a lossy film, the amplitudes are all complex quantities that can be plotted in the complex plane. Figure 1d displays the trajectories of the sums of the partial reflected waves with varying  $k$  values. The trajectories are plotted with  $r_0$  beginning at the origin, and  $r_m$  begins at the end of  $r_{m-1}$ . Since the total reflectance is the square of the module of the last trajectory in the complex plane, the total reflectance of each absorptive layer with varying  $k$  values can be readily obtained, and zero reflectance is obtained if the trajectory



returns to the origin. Figure 1d clearly shows how the reflectance evolves with varying of  $k$ . For the case of  $k = 0.4$ , the end of the trajectory almost returns to the origin, indicating the total cancellation of the partial waves with  $r_0$ .

As discussed above, the total reflectance is correlated with the total phase shift, which is also pertinent to the angle of incidence. However, the optical properties of this three-layer structure are consistent across most angles of incidence. This result occurs because the coating in this structure is much thinner than the wavelength of light ( $\sim \lambda/7n$ ) and the refraction angle in the absorptive layer remains very small over a wide range of incidence angles due to the large discrepancy in indices between the air and the absorptive layer according to Snell's law. We demonstrated this phenomenon by plotting the phase shift as a function of incident angle at a wavelength of 550 nm and with an absorptive layer thickness of 30 nm for  $s$ -polarization and  $p$ -polarization, which are shown in Fig. 1e, f. Moreover, the reflectance is smaller than 0.1 up to an angle of incidence of  $60^\circ$  for both  $s$ - and  $p$ -polarization cases (see supporting information Fig. 3S). For the case of  $p$ -polarization, there is a sharp change from  $\sim 0$  to  $\sim \pi$  in the phase shift between air and the absorptive layer ( $\phi_{12}$ ). This point corresponds to the Brewster angle ( $\theta_B = \arctan(n_t/n_i)$ ,  $n_i$  and  $n_t$  are the refractive indices of air and absorptive layer), at which no reflectance for  $p$ -polarized light can be detected from the air into the absorptive

layer. As shown in Fig. 1d, the Brewster angle is shifted to *ca.*  $70^\circ$  due to the high index of the absorptive layer, and so, the presence of the Brewster angle does not exert a significant effect on the angular dependence of the light reflection.

Herein, as a proof-of-concept experiment, we employ a CuO film to tune the reflectance of the Cu-grid lines in Cu-grid-based transparent conductive films, which in turn reduces the visibility of the grid lines when it is employed to fabricate a capacitive touch-panel sensor. Typically, the capacitive touch-panel sensor mainly consists of three layers with a dielectric optical layer sandwiched between two TCEs, which is illustrated schematically in the inset of Fig. 2. It clearly shows that the reflectance from the touch-panel sensor comprises three parts, namely, front reflection, rear reflection and substrate reflection ( $r_s$ ). The reflectance of the pure Cu film per se at  $\lambda = 550$  nm is larger than 42%; hence, high reflectance of grid lines is undesirable for pure Cu-grid TCEs used in displays and touch screens since the image quality may be degraded by the reflected light. Moreover, the larger the difference in reflectance between grid lines and substrate is, the clearer the visibility of the grid lines.

Figure 2a shows the calculated reflectivity as a function of the CuO layer thickness. The CuO/Cu structure displays a strong thickness-dependent reflectance, with a minimum value appearing in the range of thickness of 30–40 nm and a wavelength of 550–600 nm. Then, we

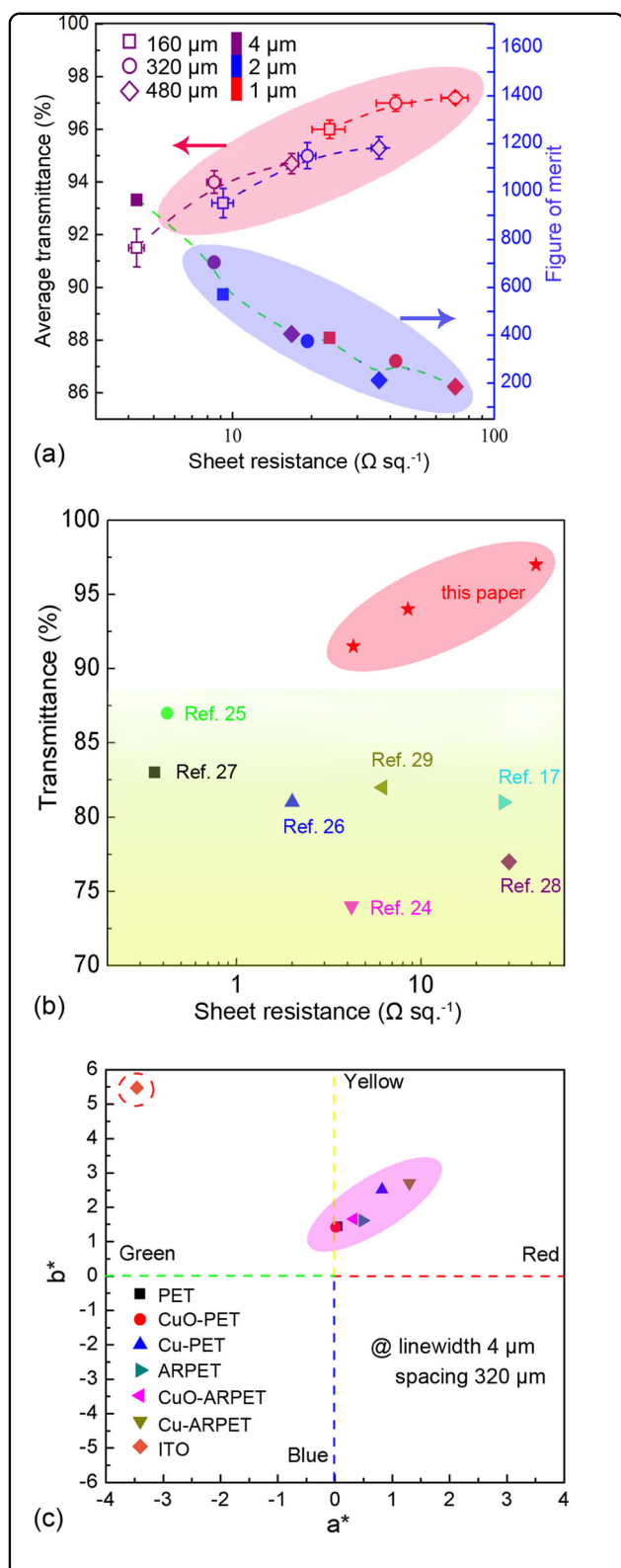


**Fig. 4 a** Plots of average transmittance ( $\lambda = 380\text{--}780 \text{ nm}$ ) vs sheet resistance for Cu-grid TCEs with various feature sizes (labeled with different colors) and grid-to-grid distances (labeled with different shapes) on ARPET substrates. All error bars show the standard deviation obtained from 10 measurements from different samples. The dotted lines are used to guide the reader's eyes. **b** Total transmittance vs sheet resistance for various transparent conductors. Our Cu-grid TCE data with a Cu layer thickness of 300 nm and state-of-the-art counterpart data for electron spun nanofibers<sup>25</sup> and nanotroughs<sup>26</sup>, nanowire/meshwire hybrids<sup>27</sup>, reduced graphene oxide-coated Cu nanowires<sup>17</sup>, graphene-coated metal mesh<sup>28</sup>, self-formed networks<sup>24</sup>, and AZO-coated metal mesh<sup>29</sup> are shown. All transmittance data in other reports are transformed to total transmittance via multiplying by 90% for a rough comparison. **c** Plot of chromaticity on the Hunter color scale for different substrates and Cu-grid TCEs with or without CuO-coating together with 300 nm ITO on PET for comparison. The grid size and spacing of the Cu grids are of 4 and 320  $\mu\text{m}$ , respectively. In the plot, + $a^*$  corresponds to red, - $a^*$  corresponds to green, + $b^*$  corresponds to yellow, and - $b^*$  corresponds to blue

fabricated a sample with a CuO thickness of 30 nm using the roll-to-roll method. Figure 2b depicts the corresponding measured and calculated reflectance spectra along with those of a pure Cu film. Excellent agreement is obtained between the experimental data and the calculation. With a 30-nm CuO coating on the Cu substrate, the reflectance at a wavelength of 550 nm is only *ca.* 2.5%, while that of the pure Cu film is *ca.* 43%. The large difference in reflectance allows for the tuning of the color of metals using these ultrathin dielectric films. As shown in the photographs (insets to Fig. 2b), the pure Cu substrate shows a typical metallic color, while the 30-nm CuO film coating on the Cu substrate creates a dark-blue color. The same results can be obtained from a 35-nm CuO film coating on the back side of a Cu substrate on PET and ARPET (see the supporting information, Fig. 4S).

Subsequently, we use this conductive sandwich structure to fabricate grid-based transparent conductive films. The fabrication of copper grids for transparent conducting electrodes (Cu grids-TCEs) is illustrated schematically in Figure 5S (see the supporting information). To fabricate displays or touch screens with high definition and high clarity, it is important to enhance the total transmittance of the TCEs. Unlike optical glass with high transmittance ( $>92\%$ ), plain PET exhibits low transmittance ( $<90\%$ ). After coating with a conductive medium, such as ITO, metal nanowires and grids, the total transmittance of the TCE is far lower than 90%, which will diminish the clarity of the resultant displays or touch screens to some extent. In this regard, two series of AR layers were designed to improve the transmittance of the PET substrate. More importantly, the feature size of the grid lines and the spacing between two grid lines can be controlled easily by varying the chemical-etching time and changing the masks with different grids configurations during the photolithographic process. Hence, tailored sheet resistance and transmittance of the Cu grids-TCEs can be easily realized.

Figure 3a and b display the photographs of a Cu-grid TCE fabricated on a flexible substrate for a 5 cm×5 cm sample and the corresponding magnified image, respectively. The grid width and spacing of the Cu grids is 4 and 320 μm, respectively. Homogeneous grids on a flexible substrate were obtained readily by using photolithography, and the corresponding AFM images of the TCEs with a line width of 4, 2 and 1 μm are shown in Figure 6S (see the supporting information). Figure 3c compares the transmittance of two Cu-grid TCEs on PET and ARPET with a feature size of 4 μm and grid-to-grid distance of 320 μm in the wavelength range from 380 to 780 nm, along with that of sputtered ITO on a PET substrate for comparison. The Cu-grid TCEs on PET exhibit a good transmittance of 85.9% at λ = 550 nm, which is comparable to ITO-based TCE. Interestingly, the Cu-grid TCEs on PET outperformed the ITO-based TCE on PET in total performance, exhibiting a flat profile over the entire visible light range in addition to some fluctuations due to the interference of a thick hard coating on both sides of the PET. After coating with AR layers on both sides of the PET, the total transmittance increases by *ca.* 8% from 85.9 to 94.3% owing to the significant enhancement in transmittance of the substrate (see the supporting information, Figure 7S). As a result, a Cu-grid TCE with a high transmittance of 94.3% and sheet resistance of 8.5 Ω sq.<sup>-1</sup> can be easily obtained. Moreover, the introduction of AR layers can significantly improve the clarity of the resultant TCEs, as displayed in Fig. 3d, e, showing the images of plants seen through Cu-grid TCEs deposited on PET and ARPET at an off-normal angle. The Cu-grid TCE on PET is slightly opaque, while that on ARPET is very clear. This noticeable difference in the image clarity demonstrates the effectiveness of the AR layers in enhancing the transmittance of the Cu-grid TCEs by suppressing the reflectance of the substrate and Cu-grid lines and, thus, eliminating the need for further coating AR layers when it is utilized to fabricate touch-panel sensors, making it more economical.

Typically, for a conductive film with a specific thickness, a smaller grid size results in a higher transmittance but a lower conductivity<sup>23</sup>. To maximize the TCE potential, it is generally required for TCEs to possess a high transmittance and conductivity. Hence, there must be a trade-off between optical transmittance and dc conductivity. The figure of merit (FOM), which is defined as the ratio of  $\sigma_{dc}/\sigma_{op}$ , is generally used to assess the performance of TCEs; the larger the FOM is, the better the TCE. The relationship among FOM ( $\sigma_{dc}/\sigma_{op}$ ), transmittance ( $T$ ) and sheet resistance ( $R_s$ ) is as follows<sup>24</sup>,

$$T = \left(1 + \frac{Z_0}{2R_s} \frac{\sigma_{op}}{\sigma_{dc}}\right)^{-2} \quad (4)$$

where  $Z_0 = 377 \Omega$  is the free space impedance,  $\sigma_{op}$  is the optical conductivity, and  $\sigma_{dc}$  is the dc conductivity of the TCEs. Here, we use the average transmittance to calculate the FOM.

Figure 4a shows the plots of average transmittance ( $\lambda = 380\text{--}780$  nm) vs sheet resistance for Cu-grid TCEs with various feature sizes ( $d = 4, 2, \text{ and } 1 \mu\text{m}$ ) and grid-to-grid spacings ( $w = 160, 320, \text{ and } 480 \mu\text{m}$ ) on ARPET substrates and the corresponding FOM data. The substrate contribution is included in all of the transmittance values. All error bars show a standard deviation of 10 measurements from different samples. For Cu-grid TCEs with a grid size of 4 μm and a grid spacing of 160 μm on an ARPET substrate, the average transmittance and the sheet resistance are 91.5% and 4.3 Ω sq.<sup>-1</sup>, respectively. By adjusting the grid size and grid spacing of the Cu-grid TCEs, the transmittance can be increased to as high as 97%, which is *ca.* 8% larger than that observed for plain PET, with a sheet resistance of 40–70 Ω sq.<sup>-1</sup>. All of the results for ARPET are superior to that of plain PET, which is shown in Figure 8S (see the supporting information).

Our Cu-grid TCEs on ARPET, with a grid size of 1–4 μm and grid spacing of 160–480 μm, exhibit excellent opto-electrical performance with very high FOMs ranging from 185 (with  $T = 97.2\%$ ,  $R_s = 71 \Omega \text{ sq.}^{-1}$ ) to 965 (with  $T = 91.5\%$ ,  $R_s = 4.3 \Omega \text{ sq.}^{-1}$ ). According to Eq. (2), the FOM is inversely proportional to the sheet resistance for a specific transmittance, and thus, the FOM can be increased largely just by increasing the thickness of the conducting film to decrease the sheet resistance without compromising the transmittance. For example, our Cu-grid TCEs on ARPET with a grid size of 4 μm, a grid spacing of 320 μm, and a Cu thickness of 300 nm exhibits a FOM of 705 ( $R_s = 8.5 \Omega \text{ sq.}^{-1}$ ,  $T = 94\%$ ). After increasing the thickness of the Cu film to 900 nm, the sheet resistance of the Cu-grid TCEs on ARPET can be lowered to  $\sim 2 \Omega \text{ sq.}^{-1}$ , and the FOM can be increased to  $\sim 3000$ . It is noteworthy that the FOMs of our Cu-grid TCEs were obtained by using the total transmittance of the conducting film (Cu grids) and substrate, rather than the conducting film alone, and the thickness of the grid lines is far thinner than that of the nanowires (which require diameters of  $>1 \mu\text{m}$  for such a low sheet resistance)<sup>25</sup>. Hence, to some extent, considering the substrate effect, the opto-electrical performances of our Cu-grid TCEs are superior to those of their state-of-the-art counterparts, such as electron spun nanofibers (87.3%,  $0.42 \Omega \text{ sq.}^{-1}$ )<sup>25</sup> and nanotroughs (81%,  $2 \Omega \text{ sq.}^{-1}$ )<sup>26</sup>, nanowire/grids wire hybrids (82.8%,  $0.36 \Omega \text{ sq.}^{-1}$ )<sup>27</sup>, reduced graphene oxide-coated Cu nanowires (81%,  $28 \Omega \text{ sq.}^{-1}$ )<sup>17</sup>, graphene-coated metal grids (77%,  $30 \Omega \text{ sq.}^{-1}$ )<sup>28</sup>, self-formed networks (73.8%,  $4.2 \Omega \text{ sq.}^{-1}$ )<sup>24</sup>, and AZO-coated metal grids (81.5%,  $6.2 \Omega \text{ sq.}^{-1}$ )<sup>29</sup>, which are shown

in Fig. 4b. This significant improvement is attributed to the substantial increase in the transmittance of the substrate after introducing two series of AR layers. Moreover, Cu-grid TCEs with various FOMs can be readily made by using a roll-to-roll MS method, a facile and high-throughput technique used in semiconducting industry.

As a replacement for ITO, the intrinsic reddish-orange color of the Cu-grid TCEs must be overcome, which is also essential for manufacturing displays with high clarity and fidelity<sup>19</sup>. Figure 4c displays the plot of chromaticity on the Hunter color scale for different substrates and Cu-grid TCEs with and without CuO coatings as well as 300 nm ITO on PET for comparison. The grid width and spacing of the Cu grids are 4  $\mu\text{m}$  and 320  $\mu\text{m}$ , respectively. This result clearly shows that the color performance of the Cu-grid TCEs is improved significantly compared with the uncoated Cu-grid TCEs after coating a thin CuO film on the Cu substrate, and the color neutrality is roughly equivalent to that of PET substrate, which is far superior to that of commercial ITO (yellow-green color shown in the upper-left corner). This difference occurs because the transmittance spectra of Cu-grid TCEs exhibit a flat profile over the entire visible light range with the exception of some fluctuations (Fig. 3b), while a peak in the transmittance of ITO appears near 550 nm (yellow-green color), which is most sensitive to the human eye. More importantly, the reflectance of the Cu film coated with 30 nm CuO has a minimum at wavelength of 550 nm, which suppresses the visibility of the grids remarkably.

In addition to the issues of the color of Cu-grid TCEs and the visibility of grid lines, coating a CuO layer on the Cu film surface can help reduce the degradation of the sheet resistance, especially in humid air and at higher temperature. The changes in the sheet resistance of Cu-grid TCEs with or without a CuO-coating layers are depicted in Figure 9Sa (see the supporting information). The grid size and spacing are of 4 and 320  $\mu\text{m}$ , respectively. The test was carried out in a humidity chamber at 60 °C with a relative humidity of 90%, which is a standard testing condition for assessing TCEs in the semiconductor industry. The pure Cu-grid TCEs show poor stability, and their performance degraded in a few days as the sheet resistance dramatically increased. This increase is attributed to the fact that pure Cu is prone to oxidation even at room temperature<sup>30</sup>, and after testing in humid conditions, a significant number of water vapor molecules are absorbed onto the surface of the Cu-grid lines and accelerate oxidation<sup>31</sup>. For CuO covered Cu-grid TCEs, the sheet resistance remained almost constant for more than 20 days, only increasing by 12%, which is lower than the standard value of 20% for TCEs in displays. We performed XPS depth measurement to characterize the compositional change after exposure to humidity at 60 °C.

The XPS depth profile of O (see the supporting information, Figure 9Sb) shows that the peaks of O 1s change similarly, and no peaks related to O are discernable at the CuO/Cu interface (~35 nm), with the exception of the profile difference on the surface due to the increase in content of hydroxides (~531.5 eV) after exposure to humidity<sup>29</sup>. These results clearly demonstrate the effectiveness of CuO in preventing the oxidation of the Cu-grid TCEs, indicating that layered CuO/Cu/CuO-grid TCEs are a superior replacement for ITO.

## Conclusions

In summary, strong interference-induced resonant light trapping in an optical cavity comprising ultrathin conductive CuO film on Cu substrate endows effective reflection suppression in ultrathin nanometer films. Since the transmittance is zero, efficient light absorption in ultrathin nanometer films can also be obtained, which may also make them an excellent candidate material for applications in solar energy conversion by balancing the trade-off between light absorption (requiring a thick film due to poor absorption), and photogenerated minority collection (requiring an ultrathin film due to poor transport properties). Moreover, the approach proposed in this study and the underlying physical mechanism can probably be extended to other metal substrates, provided that the absorptive layer with a suitable complex index is available. As a proof-of-concept experiment, a CuO film was employed to fabricate TCEs, which exhibit two functions: (1) they tune the reflectance of the Cu-grid lines in Cu-grid TCEs, which in turn reduces the visibility of grid lines when it is employed to fabricate a capacitive touch-panel sensor and (2) they prevent oxidation of the Cu grid. By optimizing the aperture and grid feature size, an excellent opto-electrical performance ( $R_s = 8.5 \Omega \text{ sq.}^{-1}$ ,  $T = 94.3\%$ ) was achieved for a given Cu thickness of 300 nm, which is superior to state-of-the-art Cu nanowires-based flexible TCEs. For a given transmittance, the sheet resistance of Cu-grid TCEs can be reduced remarkably by increasing the thickness of Cu-conducting layer. The key to the excellent performance of these Cu-grid TCEs relative to other counterparts is introducing a CuO layer to suppress the reflection of the Cu layer and to protect Cu grids from oxidation and incorporating two series of AR layers to enhance the total transmittance of TCEs. We believe that this method holds promising implications in fabricating high-performance TCEs and high-conversion efficiency solar energy absorbers.

## Acknowledgements

This work was financially supported by the National Natural Science Foundation of China (51502276, H.Y.L, and 21673053, X.L.W). We appreciate Prof Feng Pan (Tsinghua university, China) for the help on photolithography.



**Author details**

<sup>1</sup>Beijing Engineering Research Centre of Advanced Structural Transparencies for the Modern Traffic System, Beijing Institute of Aeronautical Materials, Beijing 100095, China. <sup>2</sup>CAS Key Laboratory of Nanosystem and Hierarchical Fabrication, National Center for Nanoscience and Technology, Beijing 100190, China

**Conflict of interest**

The authors declare that they have no conflict of interest.

**Publisher's note**

Springer Nature remains neutral with regard to jurisdictional claims in published maps and institutional affiliations.

**Supplementary information** is available for this paper at <https://doi.org/10.1038/s41427-018-0011-z>.

Received: 10 September 2017 Revised: 10 September 2017 Accepted: 12 December 2017.

Published online: 18 April 2018

**References**

- Cao, F. et al. Toward a high-efficient utilization of solar radiation by quad-band solar spectral splitting. *Adv. Mater.* **28**, 10659–10663 (2016).
- Singh, M. et al. Silver nanowires binding with sputtered ZnO to fabricate highly conductive and thermally stable transparent electrode for solar cell applications. *ACS Appl. Mater. Interfaces* **8**, 12764–12771 (2016).
- Gu, J. et al. Water reduction by a p-GaInP<sub>2</sub> photoelectrode stabilized by an amorphous TiO<sub>2</sub> coating and a molecular cobalt catalyst. *Nat. Mater.* **15**, 456–460 (2016).
- Sun, X. et al. Plasmon based antireflection coatings containing nanostructured Ag and silica medium. *Appl. Surf. Sci.* **258**, 3785–3788 (2012).
- Xi, J. Q. et al. Optical thin-film materials with low refractive index for broadband elimination of Fresnel reflection. *Nat. Photonics* **1**, 176–179 (2007).
- Raut, H. K. Multiscale ommatidial arrays with broadband and omnidirectional antireflection and antifogging properties by sacrificial layer mediated nanoimprinting. *ACS Nano* **9**, 1305–1314 (2015).
- Moiseev, S. G. Composite medium with silver nanoparticles as an anti-reflection optical coating. *Appl. Phys. A* **103**, 619–622 (2011).
- Spinelli, P. et al. Broadband omnidirectional antireflection coating based on subwavelength surface Mie resonators. *Nat. Commun.* **3**, 692 (2012).
- Elbahri, M. et al. An omnidirectional transparent conducting-metal-based plasmonic nanocomposite. *Adv. Mater.* **23**, 1993–1997 (2011).
- Jamali, M. et al. Photoresponsive transparent conductive metal with a photobleaching nose. *Adv. Mater.* **23**, 4243–4247 (2011).
- Kats, M. A. et al. Nanometre optical coatings based on strong interference effects in highly absorbing media. *Nat. Mater.* **12**, 20–24 (2013).
- Baran, T. et al. An efficient Cu<sub>2</sub>O photocathode for hydrogen production at neutral pH: new insights from combined spectroscopy and electrochemistry. *ACS Appl. Mater. Interfaces* **8**, 21250–21260 (2016).
- Lordan, D. et al. Asymmetric pentagonal metal meshes for flexible transparent electrodes and heaters. *ACS Appl. Mater. Interfaces* **9**, 4932–4940 (2017).
- Cheng, Y. et al. Copper nanowire based transparent conductive films with high stability and superior stretchability. *J. Mater. Chem. C* **2**, 5309 (2014).
- Guo, H. et al. Copper nanowires as fully transparent conductive electrodes. *Sci. Rep.* **3**, 2323 (2013).
- Ahn, Y. et al. Copper nanowire-graphene core-shell nanostructure for highly stable transparent conducting electrodes. *ACS Nano* **9**, 3125–3133 (2015).
- Dou, L. T. et al. Solution-processed copper/reduced-graphene-oxide core/shell nanowire transparent conductors. *ACS Nano* **10**, 2600–2606 (2016).
- Han, S. et al. Fast plasmonic laser nanowelding for a Cu-nanowire percolation network for flexible transparent conductors and stretchable electronics. *Adv. Mater.* **26**, 5808–5814 (2014).
- Rathmell, A. R. et al. Synthesis of oxidation-resistant cupronickel nanowires for transparent conducting nanowire networks. *Nano. Lett.* **12**, 3193–3199 (2012).
- Yin, Z. et al. Novel synthesis, coating, and networking of curved copper nanowires for flexible transparent conductive electrodes. *Small* **11**, 4576–4583 (2015).
- Ye, S. et al. A rapid synthesis of high aspect ratio copper nanowires for high-performance transparent conducting films. *Chem. Commun.* **50**, 2562 (2014).
- Jiang, X. et al. CuO nanowires can be synthesized by heating copper substrates in air. *Nano. Lett.* **2**, 1333–1338 (2002).
- Hecht, D. S. et al. Emerging transparent electrodes based on thin films of carbon nanotubes, graphene, and metallic nanostructures. *Adv. Mater.* **23**, 1482–1513 (2011).
- Han, B. et al. Uniform self-forming metallic network as a high-performance transparent conductive electrode. *Adv. Mater.* **26**, 873–877 (2015).
- An, S. et al. Self-junctioned copper nanofiber transparent flexible conducting film via electrospinning and electroplating. *Adv. Mater.* **28**, 7149–7154 (2016).
- Wu, H. et al. A transparent electrode based on a metal nanotrough network. *Nat. Nanotechnol.* **8**, 421–425 (2013).
- Hsu, P.-C. et al. Performance enhancement of metal nanowire transparent conducting electrodes by mesoscale metal wires. *Nat. Commun.* **4**, 2522 (2013).
- Hong, S. et al. Nonvacuum maskless fabrication of a flexible metal grid transparent conductor by low temperature selective laser sintering of nanoparticle ink. *ACS Nano* **7**, 5024–5031 (2013).
- Kim, W.-K. et al. Cu mesh for flexible transparent conductive electrodes. *Sci. Rep.* **5**, 10715 (2015).
- Im, H.-G. et al. Flexible transparent conducting hybrid film using a surface-embedded copper nanowire network a highly oxidation-resistant copper nanowire electrode for flexible optoelectronics. *ACS Nano* **8**, 10973 (2014).
- Haugrud, R. The influence of water vapor on the oxidation of copper at intermediate temperatures. *J. Electrochem. Soc.* **149**, B14 (2002).